# POSSIBILITIES OF MICROINTERFEROMETRY IN THE INVESTIGATION OF NONSTATIONARY PROCESSES

V. F. Klimkin and V. V. Pikalov

UDC 541.126

1. Introduction. The solution of a number of physical problems associated with the study of the interaction between powerful laser radiation flux and a substance (the formation of a laser spark [1], heating of a plasma obtained upon irradiation of solid targets and separate particles [2, 3]), as well as the formation of an electrical discharge in gaseous and condensed media [4, 5], requires the development of ultrarapid methods of optical recording in application to the investigation of microobjects with a characteristic dimension of $\leqslant 10^{-3}$-$10^{-2}$ cm.

The use of optical recording methods with a high time and space resolution [6] permitted the detection of details in the initial stage of electrical discharge development in liquid dielectrics at homogeneous electric field intensities of $\sim(0.3\text{-}1)\cdot 10^6$ V/cm. It has been established that the development of a discharge in a liquid dielectric has two stages in a homogeneous electric field. Investigations using a three-frame schlieren recording of the discharge dynamics showed [7] that the first ("hydrodynamic") stage is associated with processes resulting in local energy liberation near the electrode surface. Consequently, intense shocks occur and numerous initial streamers are developed. This stage is terminated by the formation of a primary ionization channel with the characteristic dimension $\leqslant 10^{-2}$ cm, which depends on the magnitude of the applied electric field and the kind of dielectric. The second stage starts with the advancement of the primary ionization channel in the form of a rapidly developing brush discharge deep in the gap, and a powerful ionization wave originates after one of the growing branches of the opposite electrode has been touched, which completes the initial stage of electrical discharge development in the liquid dielectrics.

Methods of high-speed interferometry [8] permitted a much clearer recording of divergent shocks as well as the microstructure of strong gasdynamic perturbations behind their front in the initial stage of electrical discharge development in liquid dielectrics.

The propagation of intense shocks in fluids causes abrupt and significant changes in the refractive index on the boundary of an object, which cannot permit tracking the behavior of the interference fringe during passage through the boundary of the perturbation. Hence, shocks due to perturbations which did not result in a punch-through were investigated at a sufficiently large distance from the energy liberation site in [9] in order to estimate the lower boundary of the value of the pressure and some other parameters in the energy liberation domain on the electrode surface. The restoration of the pressure profile behind the propagation shock front is also of considerable interest since it permits an independent estimation of the size of the energy liberation and pressure domain at the channel boundary.

Because of the importance of these results, their additional foundation is undoubtedly required, especially methodologically.

This paper is devoted to the further development of a new methodological approach to the investigation of the initial stage of electrical discharge formation in liquid dielectrics, proposed in [6-9], and it poses the problem of clarifying the possibilities of interferometry in application to nonstationary microperturbations with the dimension $\leqslant 10^{-2}$ cm, for which the presence of compression shocks is characteristic.

2. Experimental Setup. The diagram of the apparatus for investigating an electrical discharge in liquid dielectrics by using a Mach–Zender interferometer is represented in [8].

Since the spatial resolution of the interferometer is determined by the spacing between the fringes, it is necessary that there be several interference fringes within the limits of the object being studied. Under our conditions, when the characteristic dimension of the shocks being studied is $(1\text{-}2)\cdot 10^{-2}$ cm, the spacing between the inteference fringes was $3\cdot 10^{-3}$ cm in the plane of the object. A pulsed ruby laser was used as the source of illumination. The duration of the frame exposure was $\sim(5\text{-}7)\cdot 10^{-9}$ sec, and the time resolution was $\leqslant 5\cdot 10^{-9}$ sec.

Novosibirsk. Translated from Zhurnal Prikladnoi Mekhaniki i Tekhnicheskoi Fiziki, No. 3, pp. 14-26, May-June, 1979. Original article submitted May 10, 1978.

0021-8944/79/2003-0271$07.50  

A voltage pulse with amplitude (1-2) $\cdot 10^5$ V was delivered to the discharge chamber electrode (electrode diameter was 1 cm and the spacing between them 0.1-0.2 cm), where the chamber was filled with different fluids.

The optical diagram used in the tests permitted obtaining interference patterns of the discharge gap combined with its focused shadowgraph. The rays emerged from the limits of the optical system aperture at angles of the deviation $\geqslant 6 \cdot 10^{-2}$ rad, and a focused shadowgraph was obtained of the strong optical perturbations. An estimate of the diffraction limit of optical system resolution $\sim (1/6)\sqrt{\lambda L}$ [10] yields the quantity $\sim 10^{-4}$ cm for ray path length in the inhomogeneity under investigation, $L \sim 10^{-2}$ cm and $\lambda = 0.7 \cdot 10^{-4}$ cm. Special calibration permitted establishment that the limit (static) resolution of the recording system (taking account of the photographic material) was $\leqslant 5 \cdot 10^{-4}$ cm. Individual objects with even smaller sizes $\sim 10^{-4}$ cm were recorded on the film, but their measurement error was ~ 70%. In studying the dynamics of comparatively weak shocks being propagated at the velocity $V \sim 1.5 \cdot 10^5$ cm/sec close to the speed of sound and the frame exposure time $\sim 5 \cdot 10^{-9}$ sec, the dynamic resolution is $\sim Vt_e$, close to the limit resolution of the optical system. It should especially be noted that high spatial resolution of the recording system again permitted us to clarify the complex microstructure of strong hydrodynamic perturbations behind the front of the shocks being propagated, where the rate of process development is somewhat less.

3. Measurement Method. The change in refractive index $\Delta n(r)$ in an interferometer study of axisymmetric inhomogeneities is found from the measured displacement of the interference fringes k(x) by solving an Abel differential equation (if geometric optics is applicable and ray refraction is small)

$$k(x) = \frac{2}{\lambda} \int_x^R \frac{\Delta n(r)\, r dr}{\sqrt{r^2 - x^2}}, \tag{3.1}$$

where x is the spacing between the chord and the axis of symmetry, and R is the radius of the optical inhomogeneity in the section under investigation.

This equation is usually solved by approximate methods based on the partition of the cross section of the inhomogeneity being investigated into a number of annular zones, giving the behavior of the function $\Delta n(r)$ to be determined in each zone, and the subsequent solution of the system of algebraic equations obtained [11].

It should be noted that the procedure for solving the Abel integral equation (3.1) is among the incorrect problems of mathematical physics [12]. This means a great influence of the random error in an experimental measurement of k(x) on the error in calculating $\Delta n(r)$. Hence, the experimental curves are ordinarily smoothed by least squares [13, 14] or by representing the experimental function by a segment of a Fourier series [15]. Modern mathematical methods (regularization methods) have recently been developed [12, 16] for the solution of incorrectly posed problems, which permit the introduction of a priori constraints on the solution expected in order to diminish the influence of errors in the experimental data on the accuracy of determining the radial distribution. The method of statistical regularization, when a probabilistic method of giving the a priori information is realized [16], is compared with a number of other methods of solving (3.1) in [17], by means of a number of model functions. It is shown that inversion of the Abel equation by statistical regularization is suitable for the restoration of sufficiently complex distributions, and assures the least coefficient of amplification of the experimental measurement error. Analysis of the experience of using different methods for the Abel transformation shows [18] that the selection of any method to solve specific problems requires a special investigation on the models.

The radial distribution of the refractive index, which drops smoothly to 0 for $r_* = R$ [19], must usually be reproduced in the interferometry of plasma objects. There is comparatively little data in the literature on an analysis of the applicability of known methods of solving the Abel equation to jumplike functions, although the possible significant error in reproduction near the jump was even noted in [20]. Hence, in order to confirm the possibilities of obtaining confident results in processing shock inteference patterns, the reliability of the individual stages in the approximate solution of the Abel equation was verified in a number of model functions and experimental modeling of the method was also carried out on microobjects.

A shock in a fluid, which occurs with local energy liberation, can be represented in a first approximation in the form of a discontinuous pressure jump behind which is exponential damping [21],

$$p(r) \simeq p(R_f) \exp\left(\frac{r - R_f}{r}\right),$$

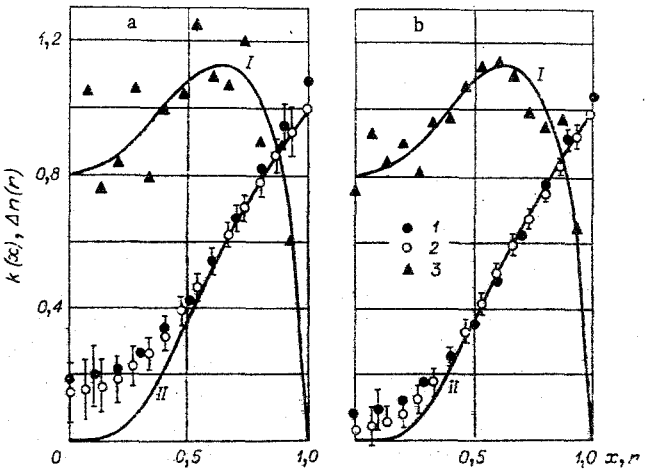


Fig. 1

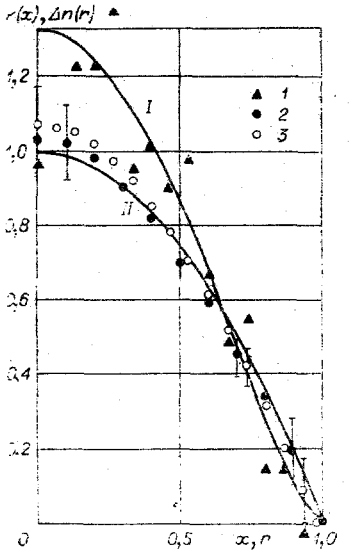


Fig. 2

where $R_f$ is the radius of the shock front. For weak shocks, where the change in temperature in the medium can be neglected, the change in the refractive index for the pressure profile under consideration has the form

$$\Delta n\,(r) \simeq A\Delta n\,(R_f)\exp\left(\frac{r-R_f}{r}\right),$$

where A is some constant. On this basis a model function with a jump on the boundary (r = R) was selected:

$$\Delta n\,(r) = \begin{cases} \exp\left(1-\dfrac{R}{r}\right), & 0 \leqslant r \leqslant R, \\ 0, & r > R. \end{cases} \tag{3.2}$$

The method of statistical regularization, which received good notices earlier for its restoration of a broad class of functions different from (3.2) [17], was used to reproduce this function. The Abel equation (3.1) was hence written in matrix form:

$$K\varphi = f, \text{ where } \varphi = n(r) - n_0 = \Delta n(r);\ f = k(x). \tag{3.3}$$

The matrix K was obtained by a parabolic approximation [19] of the function $\Delta n(r)$ in the partition zones $[r_j, r_{j+1}]$, where $j = 1, \ldots, N$. The algorithm was constructed for an arbitrary nonuniform mesh $\{r_j\}$, where $R_1 (0 \leq R_1 < R)$, $r_{N+1} = R$, which permitted reproduction of the distribution of the refractive index, when necessary, to just the external zones of the inhomogeneity.

The solution of (3.3) by the method of statistical regularization is expressed in the form [18]

$$\varphi_\alpha = (K^+WK + \alpha\Omega)^{-1}K^+Wf,$$

where $\alpha$ is found from the nonlinear equation

$$\alpha = N/[\mathrm{Sp}\,[\Omega(K^+WK + \alpha\Omega)^{-1}] + (\varphi_\alpha, \Omega\varphi_\alpha)]; \quad W_{ij} = S_i^{-2}\delta_{ij}.$$

Here $K^+$ is the transposed matrix, $W_{ij}$ is the error matrix, $\alpha$ is the regularization parameter, $\Omega$ is the Tikhonov second-order regulator [12], N is the dimensionality of the vector $\varphi$, $S_i^2$ is the variance of a random normal vector f, and $\delta_{ij}$ is the Kronecker delta. The variance of the reproduced vector $\varphi$ is determined by the relationship

$$\sigma_i^2 = (K^+WK + \alpha\Omega)_{ii}^{-1}.$$

The solution of (3.3) was sought in the class of smooth functions with a bounded second derivative. The main assumption about the behavior of the function on the boundary (r=R) was the assumption of parabolic continuation of the function $\Delta n(r)$ from the penultimate into the last zone. The actual experiment was modeled by introducing a random 3-10% normal error into the appropriate k(x).

Results of reproducing the function (3.2) by the method of statistical regularization (R=1) are presented in Fig. 1 (I is k(x) and II is $\Delta n(r)$). It is seen that the introduction of a random 10% error (Fig. 1a, points 3) from the maximum value of k results in considerable smoothing of the function in the domain $r \sim 0$. The error for reproduction of the jump is ~8% for the case of a 10 zone partition (points 1) and less than 1% for a 15 zone partition (points 2).

A diminution of the random error in measuring the shift of the interference fringes to 5% (Fig. 1b, points 3) results in a diminution in the smoothing in the central areas. The error in reproducing the jump is hence also not more than 1% for a 15 zone partition, i.e., is one-fifth the initial random error in k(x).

Since the error in the approximation is large for a small number of zones, especially in the domain where abrupt changes in the function to be reproduced are possible, and the error due to inaccurate measurement of the interference fringe shift grows with the increase in the number of zones, it is more convenient to introduce a variable-spacing partition into zones. A special program was developed to use such nonequidistant data. Results of verifying it in the model function (3.2), when the zone width diminished parabolically with the increase in the parameter x, showed that reproduction of the jump is conserved well, but smoothing in the area of $r \sim 0$ diminished somewhat [22]. Smoothing in the central zones is governed by the fact that the condition

$$d\varphi/dr|_{r=0} = 0$$

required for the Abel equation (3.1) was introduced into the algorithm.

The wave amplitude drops in going from the shock to the acoustic wave. Hence, still another model function, which drops to zero as $r \to R$,

$$\Delta n(r) = \begin{cases} 1 - \left(\frac{r}{R}\right)^2, & 0 \leqslant r \leqslant R, \\ 0, & r > R, \end{cases}$$

$$k(x) = \frac{4}{3\lambda R}\left(1 - \frac{x^2}{R^2}\right)^{3/2},$$

was selected to compare the results of the reproduction.

The results of reproducing this function by statistical regularization are represented in Fig. 2 (I is k(x) and II is $\Delta n(r)$). It is seen that the maximum error in the reproduction is around 7% (points 2 and 3 correspond to partitions into 10 and 15 zones) for an accuracy of 10% of the value of k(x) on the axis (points 1) in measuring the inteference fringe shift. The error diminishes to 3-4% for a 20 zone partition.

On the whole, sufficient confidence in the method of statistical regularization follows from the results presented, with the exception of the reproduction of the central zones of the distribution (3.2), where $\Delta n(r)$ tends to zero.

Let us examine the possible errors because of the refraction phenomenon. The light ray deviation during passage through a spherical shock is determined by the relationship

$$\varepsilon(x) = \varepsilon_1(x) + \varepsilon_2(x) \simeq \frac{2\Delta n}{n_0} \frac{x/R}{\sqrt{1-\left(\frac{x}{R}\right)^2}} + \frac{2}{n_0}\int_x^R \frac{\partial n}{\partial r}\frac{xdr}{\sqrt{r^2-x^2}}.$$

The first term is due to refraction on the surface of the shock, and the second is the deviation from the shock front because of the gradient in the refractive index.

If we select $x=0.9R$, $R\sim10^{-2}$ cm, $n_0=1.333$, $\Delta n(R)\sim10^{-3}$, then it follows from estimates that $\varepsilon_1\approx 3\cdot10^{-3}$ rad, but $\varepsilon_2\simeq 6\cdot10^{-4}$ rad for the radial distribution of the refractive index (3.2) under consideration. It is seen that the deviation of the light beams for sufficiently high values of x, even for abrupt gradients in the refractive index, is determined mainly by refraction by the shock surface. By using the relationship [23]

$$\Delta k \simeq \varepsilon^2 L/12\lambda,$$

where L is the characteristic dimension of the object, it can be shown that for angles of light deviation $\varepsilon\sim10^{-3}$ rad and $L\sim10^{-2}$ cm the refraction error is insignificant even for an accuracy of $\Delta k\sim10^{-2}$ in measuring the interference fringe shift. For instance, if $L\sim10^{-2}$ cm, then the angles of deviation at which refraction error must start to be taken into account for a fringe shift measurement accuracy of $\Delta k\sim10^{-2}$ will be $\approx 2°$, and $\Delta k\sim 0.1$ for $\varepsilon\approx 6°$. For $\varepsilon\sim6\cdot10^{-2}$ rad (half angle of the optical system aperture), the light refraction must be taken into account for measurements of the fringe shift with $\leq 4\cdot10^{-2}$ accuracy.

It should be noted that, as a rule, the maximum shift in the inteference fringes is less than one fringe when processing interference patterns of weak shocks with the dimension $\sim10^{-2}$ cm, which would require additional analysis of the accuracy in measuring the fringe shift under these conditions. Checking out the method of measuring small interference fringe shifts in the model setup in application to microobjects showed that the error in measuring the shift was $\sim 0.01$-$0.02$ fringes when using a photometric method.

However, additional errors in measuring the fringe shifts can appear in a study of dynamic objects, which is due to blurring of the interference fringes during exposure of the frame. Let us examine the influence of the finite frame exposure time on the accuracy of the interference measurements in an investigation of nonstationary processes.

The intensity distribution because of the addition of two waves when obtaining the interference pattern has the form [24]

$$I = I_1 + I_2 + 2\sqrt{I_1 I_2}\cos\delta, \tag{3.4}$$

where $I_1$, $I_2$ are the interfering wave intensities and $\delta$ is the phase difference. The contrast between the interference bands $k_b$ is defined by the relationship

$$k_b = (I_{max} - I_{min})/(I_{max} + I_{min}) = 2\sqrt{p}/(p+1), \tag{3.5}$$

where $p = I_1/I_2$. Taking account of (3.5), the expression for the intensity distribution (3.4) is written in the form

$$I = I_0(1 + k_b\cos\delta), \tag{3.6}$$

where $I_0 = I_1 + I_2$. If an (x, y) coordinate system is introduced in the plane of the screen, then the expression (3.6) for the intensity distribution can be written in the case of nonstationary objects in the form

$$I(x, y, t) = I_0\left[1 + k_b\cos\frac{2\pi}{\lambda}(y\varphi + \mu(x, t))\right], \tag{3.7}$$

where $\varphi$ is the angle between the interfering rays; $\mu(x, t)$ is the optical path difference, which is determined for axisymmetric objects by the relationship

$$\mu(x, t) = 2\int_x^R \frac{n(r, t) - n_0}{\sqrt{r^2-x^2}} rdr.$$

Since the spatial period of the fringes in the interference pattern is determined by the angle $\varphi$, i.e., $d\simeq\lambda/\varphi$, then taking this into account (3.7) is written as follows:

$$I(x, y, t) = I_0[1 + k_b\cos 2\pi(y/d + \mu(x, t)/\lambda)].$$

The intensity distribution

$$I_\tau(x, y, t_0) = \int_{t_0}^{t_0+\tau} S(t)\left[1 + k_b \cos 2\pi\left(\frac{y}{d} + \frac{\mu(x, t)}{\lambda}\right)\right] dt,$$

where S(t) is the intensity distribution of the laser pulse which satisfies the normalization condition

$$\int_{t_0}^{t_0+\tau} S(t)\, dt = I_0,$$

will be fixed on the photographic material when a pulse laser with pulse duration $\tau$ is used as the light source. In the case of a rectangular pulse shape, we obtain

$$I_\tau(x, y, t_0) = \frac{I_0}{\tau} \int_{t_0}^{t_0+\tau} \left[1 + k_b \cos 2\pi\left(\frac{y}{d} + \frac{\mu(x, t)}{\lambda}\right)\right] dt.$$

For $\tau \ll t_0$, by using the trapezoid rule we find

$$I_\tau(x, y, t_0) \simeq I_0\left[1 + k_b \cos 2\pi\left(\frac{y}{d} + \frac{\mu(x, t_0)}{\lambda} + \frac{\Delta\mu(x, t_0)}{2\lambda}\right)\cos 2\pi\frac{\Delta\mu(x, t_0)}{2\lambda}\right].$$

It hence follows that a change in the optical path difference $\Delta\mu$ during exposure results in the appearance of an additional relative shift in the interference fringe by the quantity $\Delta\mu(x, t_0)/2\lambda$ and to a diminution in the contrast to the quantity $p' = p\cos(\pi\Delta\mu(x, t_0)/\lambda)$. Expanding the function $\mu(x, t_0+\tau)$ in a Taylor series, we obtain the following expressions for the change in intensity, contrast, and phase shift:

$$\Delta I_\tau = I_\tau(x, y, t_0) - I(x, y, t_0) = \beta\tau I_0 k_b \sin 2\pi\left(\frac{y}{d} + \frac{\mu(x, t_0)}{\lambda}\right),$$

$$p' = p\cos\tau\beta, \quad \Delta\varphi = \tau\beta,$$

where $\beta = \pi\frac{\partial}{\partial t}\left(\frac{\mu(x, t)}{\lambda}\right)\Big|_{t=t_0}$, and we have for the relative shift in the interference fringes

$$\frac{\Delta\mu(x, t_0)}{\lambda} = \frac{\Delta\varphi}{2\pi} = \frac{\tau}{2}\frac{\partial}{\partial t}\left(\frac{\mu(x, t)}{\lambda}\right)\Big|_{t=t_0}. \tag{3.8}$$

To execute the estimates by means of (3.8), we introduce two optical inhomogeneity models corresponding to two different classes of physical problems. One is characteristic for plasma objects,

$$\Delta n(r) = \frac{1}{R^2}(R^2 - r^2), \quad \mu(x) = \frac{4}{3R^4}(R^2 - x^2)^{3/2}, \tag{3.9}$$

and the other for shocks,

$$\Delta n(r) = \frac{C}{R} e^{1-\frac{R}{r}}, \quad \mu(x) = 2\int_x^R \frac{\Delta n(r)\, r\, dr}{\sqrt{r^2 - x^2}}. \tag{3.10}$$

Let us assume that a linear time dependence of the displacement of the inhomogeneity boundary exists; i.e., $R = vt$, where v is the velocity of boundary expansion. We then obtain for (3.9)

$$\frac{\Delta\mu(x, t_0)}{\lambda} \simeq -\frac{2}{3}\frac{\tau}{t_0}(\lambda R)^{-1}\sqrt{1 - \left(\frac{x}{R}\right)^2}\left(1 - 4\frac{x^2}{R^2}\right) = -\frac{\tau}{t_0} g_1(x), \tag{3.11}$$

and for (3.10)

$$\frac{\Delta\mu(x, t_0)}{\lambda} \simeq -\frac{\tau}{t_0}\frac{x^2}{\lambda R^3}\int_x^R \frac{C e^{1-\frac{R}{r}}}{R\sqrt{r^2 - x^2}} r^2 dr. \tag{3.12}$$

The expression (3.11) is obtained for the domain $x \ll R$. An approximate upper bound can also be obtained for the model (3.10) if $\Delta n(r)R \leq C$. Then

$$\frac{\Delta\mu(x, t_0)}{\lambda} \lesssim -C\frac{\tau}{t_0} g_2(x),$$

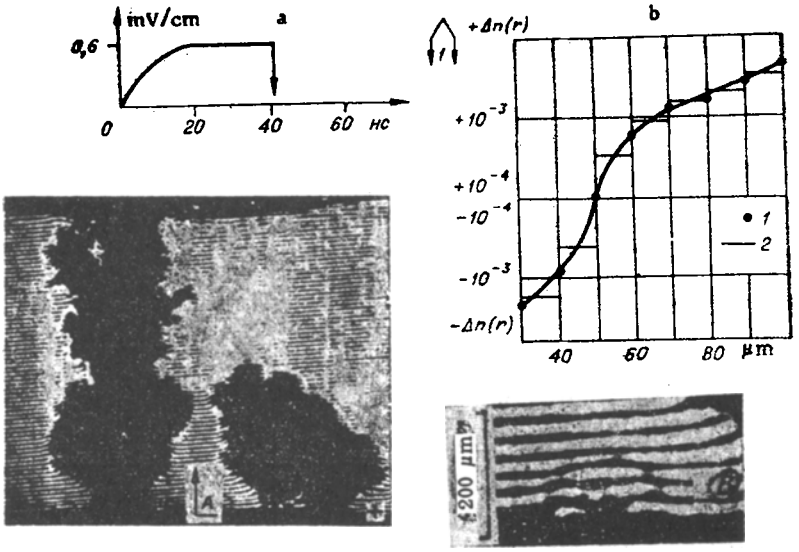


Fig. 3

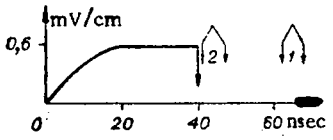


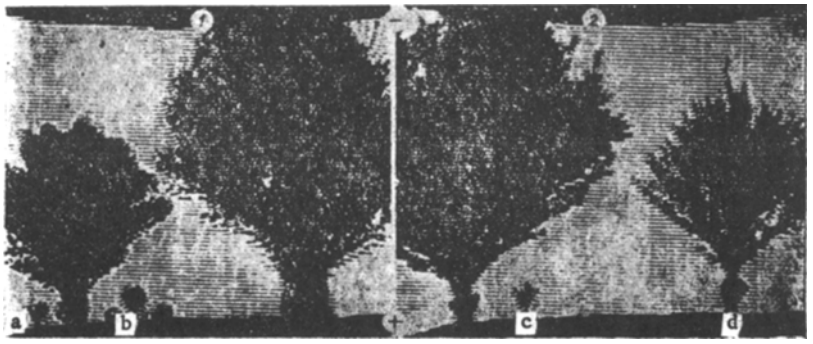


Fig. 4

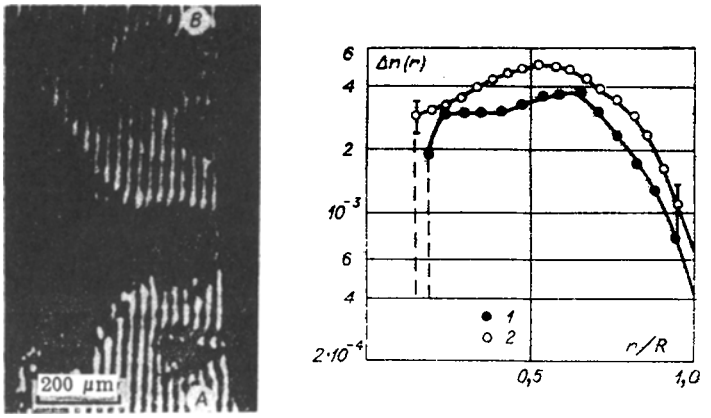


Fig. 5

where

$$g_2(x) = \frac{x^2}{2\lambda R^2}\left[\sqrt{1-(x/R)^2} + \left(\frac{x}{R}\right)^2 \ln\frac{R+\sqrt{R^2-x^2}}{x}\right].$$

Taking account of the actual profile S(t), which is closer to a Gaussian profile, permits reduction of the value of the corrections (3.11) and (3.12) by approximately half.

Estimates of the additional interference fringe shifts under the conditions of our experiments ($v \leq 2 \cdot 10^5$ cm/sec, $t_0 \simeq 5 \cdot 10^{-8}$ sec, $R \sim 10^{-2}$ cm, $\tau \simeq 5 \cdot 10^{-9}$ sec) showed that they are not more than $\sim 10^{-3}$ fringes for the plasma model. For the shock model, the additional shifts are maximal near the boundary and are $\sim 5 \cdot 10^{-3}$ fringes.

Therefore, the analysis of the influence of different factors on the accuracy of interference measurements, which has been performed, shows that the main error in the measurements will be determined by inaccuracy in measuring the interference fringe shift, which is $\sim 0.01$–$0.02$ fringes.

The possible values of the change in the refractive index $\Delta n$ for measurement of the interval was estimated by using the relationship

$$\Delta n \simeq k\lambda/L.$$

The quantity $k \sim 0.01$ fringes was determined in the range of small changes in the refractive index to the accuracy of measuring the fringe shift, while the maximal value $k \sim 1$ was constrained by the discontinuity in the interference fringe near the object boundary. Thus, e.g., for characteristic perturbations with the dimension $L \sim 10^{-2}$ cm, the range of $\Delta n$ being measured was approximately $7 \cdot 10^{-5}$–$7 \cdot 10^{-3}$.

4. Experimental Results. Typical ultrarapid frame interference patterns, obtained at different velocities, are represented in Figs. 3 and 4. The spacing between the electrodes is 0.2 cm, and the frame exposure time is $\sim 6 \cdot 10^{-9}$ sec. Spherical shocks with the radius $\sim 10^{-2}$ cm being propagated in distilled water ($\rho \sim 10^5\ \Omega \cdot$ cm) from the site of local energy liberation near the positive electrode surface, are seen in Fig. 3a. A shift in the interference fringes towards the cathode occurs on the shock front, which corresponds to an increase in the value of the refractive index as compared to its magnitude in the surrounding medium; i.e., $\Delta n > 0$. Behind the shock front the interference fringes return to approximately the previous level, or are shifted toward the anode (i.e, $\Delta n < 0$) near the local energy liberation domain.

Results of computation of the radial distribution of the refractive index behind the shock front A for the section B by the statistical regularization method are represented in Fig. 3b (points 1). Presented here for comparison are results obtained by the method of stepwise approximation [25] without the application of any smoothing procedure (2). The good agreement between the results obtained by the different methods should be noted, which confirms the high accuracy in the measurement of the interference fringe shifts, and indicates the fair possibilities of the stepwise approximation method for the reproduction of jumplike functions of the type (3.2) under these conditions.

Interference patterns exhibiting the sequence of process development in the formation of an electrical discharge in the ether ($\rho \sim 10^{10}\ \Omega \cdot$ cm) are presented in Fig. 4. Propagated from the site of local energy liberation is a shock behind whose front a "chain" of microbubbles with the characteristic dimension $\sim 10^{-3}$ cm (a, b) is seen. Ionization processes occurring behind the shock front result in the formation of a plasma channel foundation (b, c) with a complex structure, and the subsequent gap punch-through (d). In this case a cylindrical shock is seen, but the structure of the whole formation is characteristic for liquid dielectrics with a low value of the dielectric constant. Common is the primary formation of a local perturbation of cylindrical shape, from which, as a rule, a single channel distorting the electric field on the anode surface is formed successively. The magnified field domain acquires the dimension $\sim 10^{-2}$ cm, and conditions are produced for the transition "hydrodynamic" stage into a rapidly developing brush discharge (d). Results of computations of the refractive index distribution for the sections A [1) $R = 57\ \mu$m] and B [2) $R = 70\ \mu$m], performed by the statistical regularization method, are represented in Fig. 5 (the channel boundary is shown by the dashed lines).

By knowing the change in the refractive index $\Delta n(r)$, the magnitude of the density $\rho$ and the pressure p can be estimated by using the dependence of the refractive index on the density and the data on the dynamic compressibility of the medium. For example, the expression used in tests to determine the pressure behind the shock front (for $p \leq 10^3$ atm) for water has the form [26]

$$p(r) \simeq (\Delta n(r)/1.48)10^5 \text{ atm}.$$

Results of processing the interference patterns presented in Fig. 3b show that the pressure at the shock front reaches $p \simeq 270$ atm at a range of $R = 10^{-2}$ cm from the anode surface for this local perturbation.

The possible influence of defocusing on the measurement accuracy should be noted in studying microobjects; hence, as a rule, those objects which are within the sharp focusing limits on the interference patterns are subjected to processing, as is verified by the shadowgraph of the strong optical perturbations present.

Application of the method described above to investigate the dynamics of shocks in distilled water permitted obtaining quantitative results concerning the initial "hydrodynamic" stage of electrical discharge development [9] by using the approximate hydrodynamic relationships.

Results of interference measurements were compared with data obtained by using a three-frame schlieren recording system [7]. Measurements of the fundamental dynamic characteristics of the process under investigation executed by two independent methods result in consistent results for the characteristic radius of the channel, the maximal pressure, and energy density in its local liberation domain near the anode surface. The quantitative results obtained, referring to the energetics of the primary processes, can turn out to be useful in the development of a more rigorous physical model, which is extremely necessary in connection with the intensive studies in the area of producing ultrapowerful sources of energy storage.

The authors are grateful to A. G. Ponomarenko and N. G. Preobrazhenskii for aid and support in performing the research.

## LITERATURE CITED

1. M. C. Richardson and A. J. Alcock, "Subnanosecond interferometry of plasma filaments in a laser produced spark," Appl. Phys. Lett., 18, No. 8 (1971).
2. N. G. Basov, O. N. Krokhin, G. V. Sklizkov, and S. I. Fedotov, "Plasma heating and neutron generation in spherical exposure of a target to powerful laser emission," in: Lasers and Their Application [in Russian], Vol. 76, Fiz. Inst. Akad. Nauk SSSR, Moscow (1974).
3. H. Azechi, S. Oda, K. Tanaka, T. Norimatsu, T. Sasaki, T. Yamanaka, and C. Yamanaka, "Measurement of density modification of laser-fusion plasmas," Phys. Rev. Lett., 39, No. 18 (1977).
4. A. P. Alkhimov, V. V. Vorob'ev, V. F. Klimkin, A. G. Ponomarenko, and R. I. Soloukhin, "On the development of an electrical discharge in water," Dokl. Akad. Nauk SSSR, 194, No. 5 (1970).
5. A. P. Alkhimov, V. F. Klimkin, A. G. Ponomarenko, and R. I. Soloukhin, "On the development of a discharge initiated by a laser spark," in: Proc. Tenth Int. Conf. on Phenomena in Ionized Gases, Oxford (1971).
6. V. F. Klimkin, A. G. Ponomarenko, and R. I. Soloukhin, "On high-speed photorecording of the channel stage of an electrical discharge in liquid dielectrics," in: Abstracts of Reports and Communications to a Session of Section IV of the Scientific Council of the Academy of Sciences of the USSR on Theoretical and Electrophysical Problems of Energetics [in Russian], Karaganda (1976).
7. V. F. Klimkin and A. G. Ponomarenko, "Multiframe system for optical photorecording of initial stages in the development of ultrarapid processes," in: Questions of Gasdynamics [in Russian], Inst. Teor. Prikl. Mat. Sib. Otd. Akad. Nauk SSSR, Novosibirsk (1975).
8. V. F. Klimkin, A. V. Melekhov, A. G. Ponomarenko, and R. I. Soloukhin, "Ultrafast interferometry of the initial stage of electrical discharge development in liquid dielectrics," in: Questions of Gasdynamics [in Russian], Inst. Teor. Prikl. Mat. Sib. Otd. Akad. Nauk SSSR, Novosibirsk (1975).
9. V. F. Klimkin and A. G. Ponomarenko, "Investigation of pulse electrical punchthrough of fluids by using optical interferometry," Preprint No. 4, Inst. Teor. Prikl. Mat. Sib. Otd. Akad. Nauk SSSR (1978).
10. G. V. Sklizkov, "Lasers in high-speed photography," in: Laser Handbook. North-Holland, Amsterdam (1972).
11. R. U. Ladenburg, in: Physical Measurements in Gasdynamics and Combustion [Russian translation], IL, Moscow (1957).
12. A. N. Tikhonov and V. Ya. Arsenin, Methods of Solving Incorrect Problems [in Russian], Nauka, Moscow (1974).
13. K. Bockasten, "Transformation of observed radiances into radial distribution of the emission of a plasma," J. Opt. Soc. Am., 51, No. 9 (1961).
14. L. T. Lar'kina, "On the computation of the radial emissivity distribution," in: Plasmatron Application in Spectroscopy [in Russian], Ilim, Frunze (1970).
15. M. Kock and J. Richter, Der Einfluss statistischer Messfehler auf die Lösung einer Abelschen Integralgleichung," Ann. Phys., 24, No. 1, 30 (1969).

16. V. F. Turchin, V. P. Kozlov, and M. S. Malkevich, "Use of mathematical statistics methods to solve incorrect problems," Usp. Fiz. Nauk, 102, No. 3 (1970).
17. V. V. Pikalov and N. G. Preobrazhenskii, "On the Abel transformation for holographic interferometry of a point explosion," Fiz. Goreniya Vzryva, No. 6 (1974).
18. V. V. Pikalov and N. G. Preobrazhenskii, "On some problems of low-temperature plasma diagnostics solved by using an electronic computer," in: Properties of a Low-Temperature Plasma and Diagnostic Methods [in Russian], Nauka, Novosibirsk (1977).
19. V. A. Gribkov, V. Ya. Nikulin, and G. V. Slizkov, "Method of two-beam interferometer investigation of axisymmetric dense plasma configurations," Kvantovaya Elektron., No. 6 (1971).
20. J. Winckler, "The Mach interferometer applied to studying an axially symmetric supersonic air jet," Rev. Sci. Instrum., 19, No. 5 (1948).
21. R. Cole, Underwater Explosions [Russian translation], IL, Moscow (1950).
22. V. F. Klimkin and V. V. Pikalov, "On interferometer recording of microexplosive processes in a fluid," in: Mechanics of Explosive Processes [in Russian], Inst. Gidrodinamika Sib. Otd. Akad. Nauk SSSR, Novosibirsk (1977).
23. F. C. Jahoda, E. M. Little, W. E. Quinn, F. L. Ribe, and G. A. Sawyer, "Plasma experiments with a 570 kJ theta-pinch," J. Appl. Phys., 35, No. 8 (1964).
24. M. Born and E. Wolf, Principles of Optics, Pergamon (1975).
25. S. A. Abrukov, Shadow and Interference Methods of Investigating Optical Inhomogeneities [in Russian], Kazan (1962).
26. V. F. Klimkin, V. V. Pikalov, and K. A. Tinchurin, "Application of interferometry to investigate divergent shocks in fluids," in: Physical Gasdynamics [in Russian], Inst. Teor. Prikl. Mat. Sib. Otd. Akad. Nauk SSSR, Novosibirsk (1976).

# DESTRUCTION OF COARSE AND FINE WATER DROPS BY MONOPULSES OF A RUBY LASER

V. I. Novikov and V. N. Pozhidaev

UDC 535.21

In addition to the known method of evaporating water drops in the intensive radiation field of a $CO_2$ laser, papers have recently appeared wherein the destruction of water drops without the conversion of the light energy they absorbed into heat is investigated (surveys [1, 2], for example). Papers devoted to nonthermal methods of destroying a water aerosol, although still few in number, indicate the proposal of three methods of destroying the drops: optical breakdown in water, excitation of mechanical vibrations of the drops, and photochemical destruction of the water molecules [1, 2]. The optical breakdown phenomenon, when intense destructive shocks occur in a water drop subjected to a laser monopulse, has been investigated more fully than the other methods but also clearly insufficiently. Experiments on destroying millimeter- and micron-sized drops by ruby laser monopulses are described in this paper, values of the parameters characterizing this process are determined, and an approximate estimate of the energy and power of the laser pulses required to destroy a water aerosol in a track of definite length is also given.

1. Experimental Investigation of the Destruction of Coarse Water Drops. The effect of monopulse laser radiation on a suspended water drop of ~2 mm radius was observed in the experiments. The diagram of the apparatus is presented in Fig. 1. The gigantic pulse from a OGM-20 ruby laser 2 was focused at the center of the drop 4 suspended from the capillary 1 by using a lens with a 5-cm focal length 3. By using a plane-parallel divider plate 5 and the collector lens 6, a part of the radiation is sent off to the IKT-1M calorimeter 7 to measure the pulse energy. The pulse duration of the ruby laser was ~20 nsec at the half-power level, the maximum energy per pulse was ~0.5 J, and the area of the focal spot in air, determined by the hole pierced in foil, was about $2.8 \cdot 10^{-3}$ cm$^2$.

Moscow. Translated from Zhurnal Prikladnoi Mekhaniki i Tekhnicheskoi Fiziki, No. 3, pp. 26-35, May-June, 1979. Original article submitted March 29, 1978.

 0021-8944/79/2003-0280$07.50 